RESEARCH ARTICLE

The hERG potassium channel intrinsic ligand regulates N- and C-terminal interactions and channel closure

Sara J. Codding and Matthew C. Trudeau (ORCID)

Human ether-à-go-go–related gene (hERG, KCNH2) voltage-activated potassium channels are critical for cardiac excitability. hERG channels have characteristic slow closing (deactivation), which is auto-regulated by a direct interaction between the N-terminal Per-Arnt-Sim (PAS) domain and the C-terminal cyclic nucleotide binding homology domain (CNBHD). hERG channels are not activated by the binding of extrinsic cyclic nucleotide ligands, but rather bind an "intrinsic ligand" that is composed of residues 860–862 within the CNBHD and mimics a cyclic nucleotide. The intrinsic ligand is located at the PAS–CNBHD interface, but its mechanism of action in hERG is not well understood. Here we use whole-cell patch-clamp electrophysiology and FRET spectroscopy to examine how the intrinsic ligand regulates gating. To carry out this work, we coexpress PAS (a PAS domain fused to cyan fluorescent protein) in trans with hERG "core" channels (channels with a deletion of the PAS domain fused to citrine fluorescent protein). The PAS domain in trans with hERG core channels has slow (regulated) deactivation, like that of WT hERG channels, as well as robust FRET, which indicates there is a direct functional and structural interaction of the PAS domain with the channel core. In contrast, PAS in trans with hERG F860A core channels has intermediate deactivation and intermediate FRET, indicating perturbation of the PAS domain interaction with the CNBHD. Furthermore, PAS in trans with hERG L862A core channels, or PAS in trans with hERG F860G,L862G core channels, has fast (nonregulated) deactivation and no measurable FRET, indicating abolition of the PAS and CNBHD interaction. These results indicate that the intrinsic ligand is necessary for the functional and structural interaction between the PAS domain and the CNBHD, which regulates the characteristic slow deactivation gating in hERG channels.

Introduction

Human ether-à-go-go (EAG)–related gene (hERG, KCNH2) channels are critical for repolarization of cardiac action potentials (Sanguinetti and Jurkiewicz, 1990; Sanguinetti et al., 1995; Trudeau et al., 1995), and mammalian EAG-related gene channels are also expressed in the brain (Guasti et al., 2005) and in tumor cells (Bianchi et al., 1998). hERG channels are targets for heart disease since inherited mutations in the hERG gene cause type 2 long QT syndrome, and the off-target effects of pharmaceuticals and other drugs inhibit hERG channel currents and cause acquired long QT syndrome, a common clinical problem (Curran et al., 1995; Sanguinetti et al., 1995; Trudeau et al., 1995).

Voltage-activated potassium channels in the KCNH family include hERG, EAG, and EAG-like (ELK) channels (Warmke and Ganetzky, 1994). Like other voltage-activated K channels, KCNH subunits have six transmembrane domains and intracellular N- and C-terminal domains (Warmke and Ganetzky, 1994; Fig. 1, A and B). Four individual subunits assemble to form tetramers with a central pore (Wang and MacKinnon, 2017; Fig. 1 C). Unlike other voltage-activated K channels, each KCNH channel subunit has an N-terminal Per-Arnt-Sim (PAS) domain and a C-terminal cyclic nucleotide–binding homology domain (CNBHD; Warmke and Ganetzky, 1994; Morais Cabral et al., 1998; Fig. 1, A–D). Here, for clarity, we refer to the first 135 amino acids of hERG as the PAS domain, as suggested in a recent review (Morais-Cabral and Robertson, 2015). The first 135 amino acids of hERG are alternatively known as an "eag domain" (Morais Cabral et al., 1998), composed of a PAS-CAP that "caps" the PAS domain, and which includes residues 1–25, and the PAS domain, which encodes residues 26–135 (Gustina and Trudeau, 2012). The KCNH CNBHD is homologous to the cyclic nucleotide–binding domain (CNBD) of both the cyclic nucleotide–gated (CNG) and hyperpolarization-activated cyclic nucleotide–regulated (HCN) channels (Guy

Department of Physiology, University of Maryland School of Medicine, Baltimore, MD.

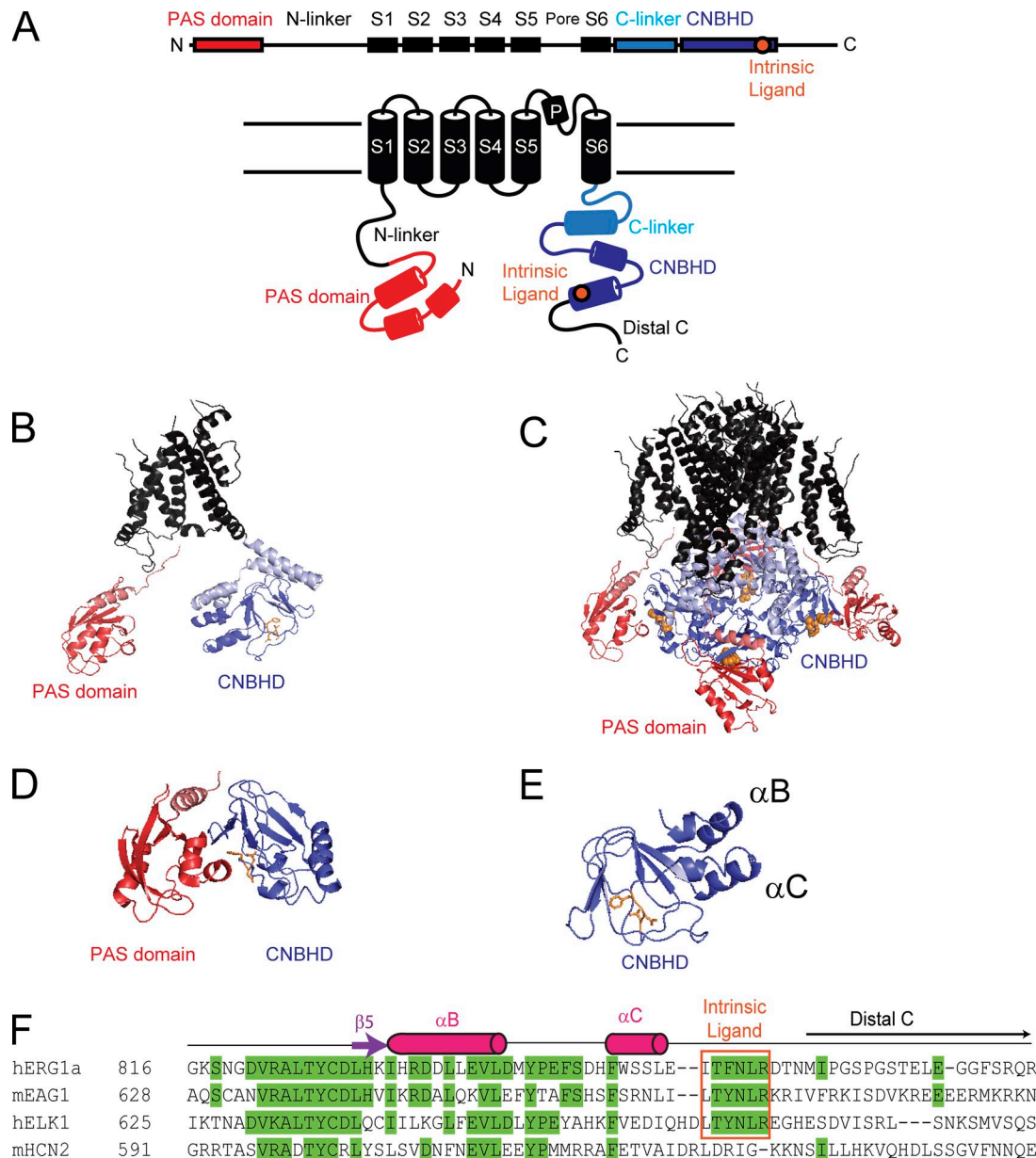Correspondence to Matthew C. Trudeau: mtrudeau@som.umaryland.edu.

Figure 1. **Schemes and models of hERG channels. (A)** Schematic of a single hERG channel subunit with six transmembrane (S1–S6) domains, a pore (P) domain that forms the ion conduction pathway and intracellular N- and C-terminal regions. hERG (and other KCNH channels) have an N-terminal PAS domain and a C-terminal CNBHD. The CNBHD contains an intrinsic ligand motif (orange circle). **(B)** Cryo-EM structure of a single hERG subunit, showing the site of the intrinsic ligand (orange) in the CNBHD (PDB accession no. 5VA2). **(C)** Cryo-EM structure of a hERG tetramer, showing intersubunit PAS and CNBHD interactions and showing location of intrinsic ligands (orange; PDB accession no. 5VA2). **(D)** X-ray crystal structure of PAS-CNBHD of KNCH1 (EAG) channels, showing intrinsic ligand (orange) at the PAS domain-CNBHD interface (PDB accession no. 4LLO). **(E)** Cryo-EM structure of the hERG CNBHD with the intrinsic ligand (orange; PDB accession no. 5VA2). **(F)** Structurally guided alignment of part of the CNBHD (β roll 5, α B helix, α C helix and the intrinsic ligand) and distal C-terminal region of KCNH family members hERG, mEAG1, and hELK1 with the CNBD of HCN2 channels. Intrinsic ligand residues are within the red box, as indicated (structural alignment: hERG, PDB accession no. 5VA2; mEAG, PDB accession no. 4LLO; and mHCN2, PDB accession no. 3ETQ; and the hELK sequence is included and primary sequence alignment is structurally guided by zElk, PDB accession no. 3UKN).

et al., 1991; Warmke et al., 1991; Zagotta et al., 2003). CNG and HCN channels are activated by the direct binding of cyclic nucleotides (Zagotta et al., 2003), but KCNH channels are not directly activated by cyclic nucleotides (Robertson et al., 1996; Brelidze et al., 2009). Instead, KCNH channels have an "intrinsic ligand" that is formed by a few conserved amino acids located distal to the α C helix in the CNBHD (Fig. 1, E and F; Brelidze et al., 2012, 2013). The intrinsic ligand mimics a cyclic nucleotide and binds

KCNH channels in an analogous position as a cyclic nucleotide in the CNBD of CNG or HCN channels (Brelidze et al., 2012, 2013; Morais-Cabral and Robertson, 2015; James and Zagotta, 2017).

The role of the intrinsic ligand in hERG gating is not clear. The principal part of the hERG intrinsic ligand motif is composed of three amino acids, phenylalanine, asparagine, and leucine (FNL), at positions 860–862 in the CNBHD (Fig. 1 F), where residues F860, N861, and L862 occupy a hydrophobic pocket in the β-roll

of the CNBHD (Fig. 1 E). hERG channels with point mutations F860A or L862A have an accelerated time course of deactivation gating (Brelidze et al., 2013). In ELK channels, the intrinsic ligand motif is composed of residues tyrosine, asparagine, and leucine (YNL) at positions 740–742 (Fig. 1 F), and mutations in the intrinsic ligand disrupt voltage-dependent potentiation of channel gating (Brelidze et al., 2013; Dai and Zagotta, 2017). A fluorescent noncanonical amino acid introduced into the ELK intrinsic ligand at N741 is quenched by a nearby transition metal bound to di-histidine residues in either the PAS or the CNBHD in a voltage-dependent manner, indicating that the PAS moves in relation to the CNBHD and the intrinsic ligand moves relative to the CNBHD during voltage-dependent potentiation (Dai and Zagotta, 2017; Dai et al., 2018; Khoo and Pless, 2018). In mammalian EAG channels, the intrinsic ligand is a YNL motif (Fig. 1 F), and dual point mutations at Y699 and L701 perturb activation gating and disrupt the characteristic Cole–Moore effect, which is a voltage dependence of populating closed states in the activation pathway (Zhao et al., 2017). Thus, the intrinsic ligand appears to regulate diverse gating functions in KCNH channels.

In addition to the intradomain interactions of the intrinsic ligand motif with the β roll of the CNBHD, structures suggest that the main chain backbone of the intrinsic ligand motif resides at the buried interface of the interdomain PAS–CNBHD interaction (Fig. 1 C) that is found in neighboring hERG subunits (Gustina and Trudeau, 2011; Gianulis et al., 2013; Wang and MacKinnon, 2017). This interdomain PAS–CNBHD interaction is also found in mammalian EAG channels (Fig. 1 D) and is likely a defining feature in the KCNH family of channels (Haitin et al., 2013; Whicher and MacKinnon, 2016). The hERG PAS–CNBHD interaction regulates the characteristically slow deactivation gating in hERG (Gustina and Trudeau, 2011; Gianulis et al., 2013). Deletion of either the PAS or the CNBHD disrupts (i.e., markedly speeds up) deactivation of hERG channels (Gustina and Trudeau, 2011, 2012; Gianulis et al., 2013). Functional and structural determinants of the PAS–CNBHD interaction that reside in the PAS domain (e.g., residues Y43 and R56) have been identified (Morais Cabral et al., 1998; Gustina and Trudeau, 2009; Gianulis and Trudeau, 2011; Wang and MacKinnon, 2017), but residues in the CNBHD that are functionally critical for the PAS–CNBHD interaction are not known.

Here we show that the intrinsic ligand is required for the PAS–CNBHD interaction that regulates characteristic slow deactivation gating in hERG channels. We report that individual mutations at the FNL motif (F860A and L862A) or a double mutant (F860G,L862G) perturb (i.e., speed up) deactivation gating as measured with electrophysiology and disrupt the structural interaction between the PAS domain and the channel as measured with FRET spectroscopy.

Materials and methods
Reagents
All isolated PAS domains used in the experiments here had a cyan fluorescent protein (CFP) fused at the C terminus, and all hERG channels or hERG channels with a deletion of the PAS domain (hERGΔPAS channels) had a citrine fused to the C terminus. For

clarity of presentation, hERG PAS-CFP domains are referred to as PAS domains and hERG ΔPAS-citrine channels are referred to as hERG core channels in the Results and Discussion sections. Point mutants in the hERG intrinsic ligand (F860A, L862A, or the double mutant F860G,L862G) were generated using oligo-based mutagenesis by a custom commercial service (BioInnovatise). The hERG PAS domain–CFP complementary DNA (cDNA) and the hERGΔPAS–citrine cDNA were previously described (Gustina and Trudeau, 2009; Gianulis et al., 2013). All hERG channels in this study contained the S620T mutation, which markedly diminished rapid inactivation, to better measure deactivation gating in isolation from inactivation gating and which we have used previously (Herzberg et al., 1998; Gustina and Trudeau, 2009; Gianulis et al., 2013). Human embryonic kidney (HEK293) cells were transiently transfected per the manufacturer's protocol (Mirus Bio) with 1–1.5 µg of hERG cDNAs. For coexpression experiments, hERG-PAS-CFP and hERGΔPAS–citrine cDNAs were transfected at a 3:1 ratio. In this study, we used a monomeric version of CFP and citrine, both of which we used previously (Gustina and Trudeau, 2009; Gianulis et al., 2013).

Fluorescence image acquisition
Fluorescence imaging experiments were performed on an inverted microscope (Nikon TE-2000). Cells were imaged with a Nikon 60× objective with a numerical aperture of 1.45. Cells were illuminated with a 120-W X-Cite lamp (Lumen Dynamics). Spectra for FRET analysis were gathered using two filter cubes: (1) a custom FRET cube (436/20, 455dclp, D460lp) and (2) a YFP cube (HQ500/20, Q515lp, HQ520lp), both from Chroma Technology. Light was passed to a Spectra Pro 2150i spectragraph (Princeton Instruments) to generate line spectra. Images were recorded using a coupled-charge device camera (Cascade 512B) and MetaMorph image acquisition and analysis software (Molecular Devices). Background was determined from a blank area of each image and was subtracted during analysis.

Calculation of FRET
FRET was measured using a spectral separation method (Selvin, 1995) that we have used in previous studies (Trudeau and Zagotta, 2004; Gustina and Trudeau, 2009, 2013; Liu and Trudeau, 2015; Jones et al., 2018). The spectral method is advantageous as it controls for variations in the ratio of the donor (CFP) to the acceptor (citrine). It eliminates variability errors in the quantum yield of the acceptor and allows for correction of the small but finite direct excitation of the acceptor by light used to excite the donor. From analysis of line spectra from each cell, we determined Ratio A – Ratio A_0, a value proportional to FRET efficiency (Fig. 2).

First, Ratio A_0, which is a control measure of direct excitation of the acceptor by 436 nm light, was calculated from control cells expressing hERG-citrine channels (Fig. 2, A and C). We measured the emission spectrum using a custom FRET cube resulting from direct excitation by 436 nm light (Fig. 2 C, red trace, F^{436}_{direct}) and emission spectrum using a YFP cube from excitation by 500 nm light (Fig. 2 C, green trace F^{500}) and calculated the ratio of the intensity of F^{436}_{direct} and F^{500} to solve Ratio A_0.

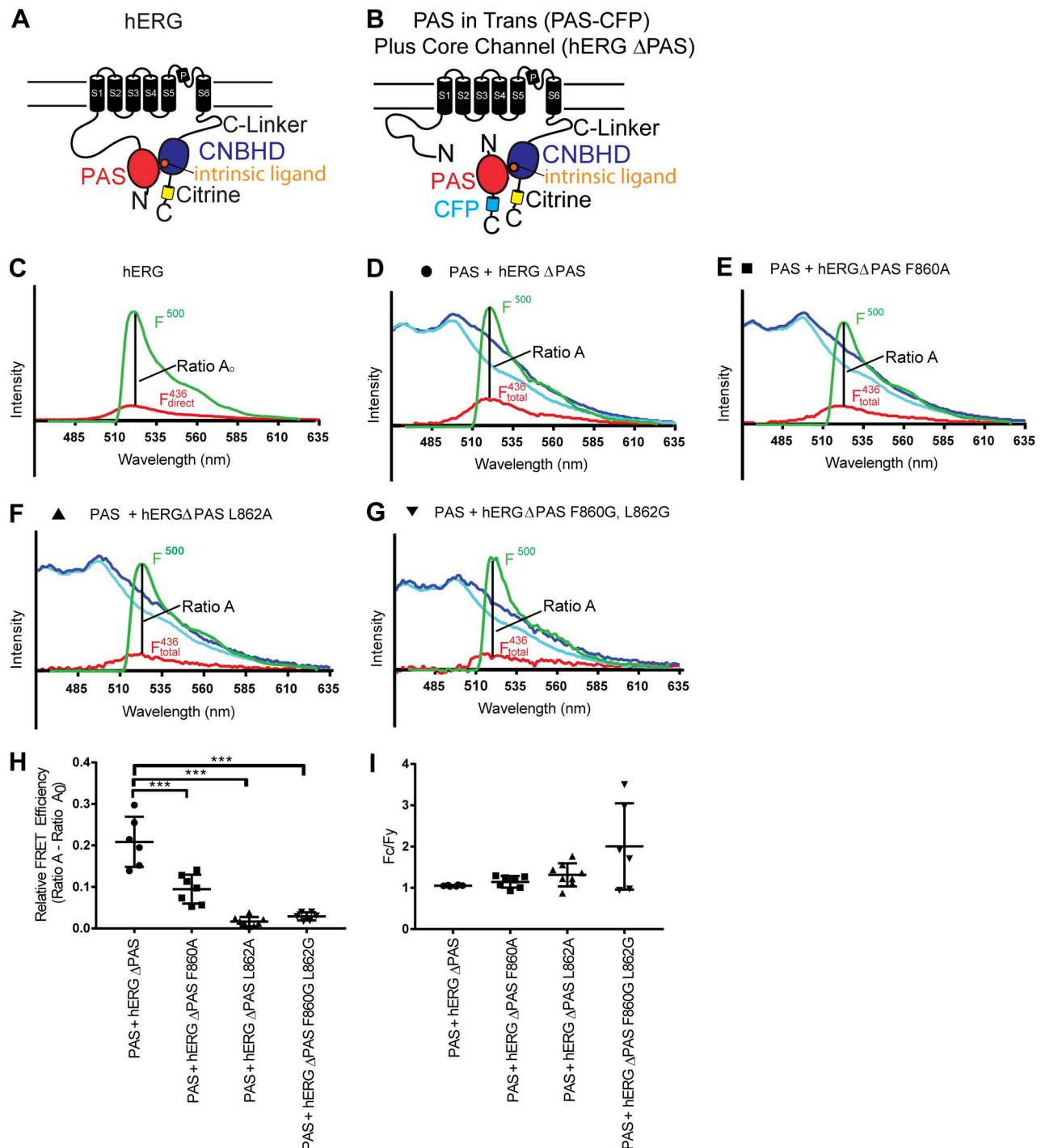$$\text{Ratio } A_0 \;=\; F^{436}_{direct}/F^{500}. \tag{1}$$

Figure 2. **Mutations in the intrinsic ligand disrupted a structural interaction between the PAS domain and the CNBHD as measured with FRET spectroscopy. (A and B)** Schematics of WT hERG subunit (A) and the PAS domain in trans with hERG core channels (B). **(C)** Line spectra plotted as intensity in arbitrary units versus wavelength (nm) from a control cell expressing WT hERG fused to citrine. Red trace (F^{436}_{direct}) is the emission spectra from the FRET cube, and green trace (F^{500}) is the emission spectra from the YFP cube. Ratio A_0 is the ratio of intensities of F^{436}_{direct}/F^{500} (see Materials and methods). **(D)** Emission spectra from positive control cell expressing PAS in trans with hERG core channels in which the dark blue trace is emission from the FRET cube, the cyan trace is a scaled control CFP spectrum, and the red trace (F^{436}_{total}) is calculated by subtracting the cyan from the dark blue trace. The green trace (F^{500}) is the emission spectrum from the YFP cube. Ratio A is the ratio of intensities of F^{436}_{total}/F^{500}. **(E–G)** Spectra from cells containing PAS domains in trans with mutant hERG core channels, PAS in trans with hERG F860A core channels (E), PAS in trans with hERG L862A core channels (F), and PAS in trans with hERG F860G,L862G core channels (G). **(H)** Scatter plot of relative FRET efficiency, Ratio A – Ratio A_0, from data in C–G. **(I)** Scatter plot of Fc/Fy, which is the relative ratio of CFP emission (Fc) to citrine emission (Fy). Each point is from a different cell. The long horizontal lines are the mean and the shorter lines are the SD in H and I. Statistical significance is indicated as ***, P < 0.001 by one-way ANOVA and Tukey's post hoc test.

Second, we determined Ratio A from cells coexpressing PAS in   trans with hERG core channels (Fig. 2, B and D) and PAS in trans

with hERG core channels with mutations in the intrinsic ligand (Fig. 2, E–G). Emission spectra from CFP fused to PAS and citrine fused to hERG core channels was measured following excitation at 436 nm using the custom FRET cube (Fig. 2, D–G, dark blue trace). A subtracted spectrum (Fig. 2, D–G, F^{436}_{total}, red trace) was generated by subtracting a scaled CFP spectrum from a control cell expressing PAS (Fig. 2, D–G, cyan trace) from the CFP and citrine emission trace (dark blue trace). The subtracted spectrum (Fig. 2, D–G, F^{436}_{total}, red trace) contains a FRET component, F^{436}_{FRET}, and a component due to the direct excitation of citrine by 436 nm light, F^{436}_{direct}. The F^{436}_{total} spectrum was normalized to the emission from the YFP cube (Fig. 2, D–G, F^{500}, green trace) to generate Ratio A.

$$\text{Ratio A} = F^{436}_{total}/F^{500} = F^{436}_{FRET}/F^{500} + F^{436}_{direct}/F^{500}. \quad (2)$$

Third, to calculate the FRET component, F^{436}_{FRET}/F^{500}, we determined Ratio A – Ratio A_0, which is proportional to FRET efficiency and decreases as FRET decreases and increases as FRET increases, and was determined by substituting Eq. 1 into Eq. 2:

$$\text{Ratio A} - \text{Ratio A}_0 = (F^{436}_{FRET}/F^{500} + F^{436}_{direct}/F^{500}) - F^{436}_{direct}/F^{500} = \quad (3)$$
$$F^{436}_{FRET}/F^{500}.$$

The FRET component, F^{436}_{FRET}/F^{500}, is equal to Ratio A – Ratio A_0, is proportional to FRET efficiency, and is plotted in Fig. 2 H.

Calculation of Fc/Fy

The value Fc/Fy is the fluorescence intensity of the donor (CFP) divided by the fluorescence intensity of the acceptor (YFP or, in this study, citrine) at the peak emission wavelength. Fc/Fy ratios serve as an independent measure of the relative amount of donor to acceptor. An Fc/Fy ratio that is similar among different experiments means that the relative donor-to-acceptor ratio was similar. The observed CFP fluorescence is measured to obtain Fc, but in experiments with FRET, the observed CFP fluorescence is artificially reduced due to transfer of energy to citrine. This FRET-associated CFP signal reduction was corrected here as previously described (Erickson et al., 2001; Zheng and Zagotta, 2004; Gustina and Trudeau, 2009). The FRET ratio (FR) was calculated as

$$\text{FR} = \text{Ratio A}/\text{Ratio A}_0 = 1 + (F436_{FRET}/F436_{direct}). \quad (4)$$

The effective FRET efficiency (E_{eff}) was calculated as

$$E_{eff} = (\varepsilon\text{citrine}_{436}/\varepsilon\text{CFP}_{436})(\text{FR} - 1). \quad (5)$$

The constants $\varepsilon\text{citrine}_{436}$ and $\varepsilon\text{CFP}_{436}$ are the molar extinction coefficients for citrine and CFP, respectively (Shaner et al., 2005; Rizzo et al., 2006). The true CFP emission (Fc) was then calculated as

$$F_{CFP\_true} = F_{CFP\_observed}/(1 - E_{eff}) \quad (6)$$

and reported as Fc and divided by Fy in the Fc/Fy plot (Fig. 2 I).

Electrophysiology

Whole-cell patch clamp was performed on an inverted microscope (Nikon TE-2000) with an EPC 10 patch clamp (HEKA Instruments) and Patchmaster Software (HEKA Instruments) as described previously (Gianulis et al., 2013). The external (bath) solution was (in mM) 137 NaCl, 4 KCl, 1.8 CaCl$_2$, 1 MgCl$_2$, 10 glucose, 5 TEACl, and 10 HEPES, pH 7.4. The internal (pipette) solution was (in mM) 130 KCl, 1 MgCl$_2$, 5 EGTA, 5 MgATP$_2$, and 10 HEPES, pH 7.2 Patch pipettes had initial resistances of 2–4 MΩ. HEK293 cells were recorded from 24–72 h following transfections. All recordings were performed at room temperature (22 ± 2°C).

Analysis of ionic currents

The conductance–voltage relationships (Fig. 4) were fit with a Boltzmann function. Deactivation was determined from double exponential function fits to the inward "tail current" at –100 mV (Fig. 3, C–N) and reported in a scatter plot (Fig. 5, A and B) and in Table 1. The half time to activation is the time at which the current at 60 mV reached half of its maximum value (Fig. 5 C).

Statistical analysis

The data are reported as the mean ± SD unless otherwise noted. Time constants of deactivation and Ratio A – Ratio A_0 were plotted as scatter plots using statistical software (GraphPad Prism). Means were compared by one-way ANOVA (GraphPad Prism), and statistical significance was assigned using Tukey's post hoc t test.

Results

We examined hERG channels (Fig. 2 A) in which we coexpressed PAS (isolated hERG PAS domains fused to CFP) in trans with core hERG channels (hERGΔPAS channels fused to citrine; Fig. 2 B) in HEK293 cells. We performed fluorescence imaging to measure spectra (Fig. 2, C–G) and used ratiometric analysis to determine Ratio A – Ratio A_0 (Fig. 2 H), which is proportional to FRET efficiency. As CFP and citrine are FRET pairs, this assay reports a structural interaction between the PAS domain and the core hERG channel (Gianulis et al., 2013). The control Ratio A_0 (Eq. 1) was determined by taking the ratio of the emission spectra from cells expressing control hERG-citrine channels (Fig. 2 A) using a FRET cube (F^{436}_{direct}, red line, Fig. 2 C) and a YFP cube (F^{500}, green line, Fig. 2 C; also see Materials and methods). We determined Ratio A (Eq. 2) by measuring emission spectra from cells expressing PAS in trans with hERG core channels or PAS in trans with hERG core channels containing intrinsic ligand mutations using a FRET cube (dark blue line, Fig. 2, D–G) and subtracting a separate CFP control spectrum (cyan trace, Fig. 2, D–G), which results in a subtracted spectrum (F^{436}_{total}, red trace Fig. 2, D–G) normalized to the emission spectra from a YFP cube (F^{500} green trace Fig. 2, D–G). Next, we calculated Ratio A – Ratio A_0 (Eq. 3) for positive control PAS in trans with hERG core channels and found a value of 0.20 ± 0.06 (Fig. 2 H), which is a robust measure of FRET and indicates the proximity of the PAS domain and the channel core.

In contrast to the positive controls, PAS in trans with hERG F860A core channels had a smaller Ratio A – Ratio A_0 of 0.09 ± 0.06, which indicated reduced FRET (Fig. 2, E and H). PAS in trans with hERG L862A core channels (Fig. 2 F) or PAS in trans with hERG F860G,L862G core channels (Fig. 2 G) both had a Ra-
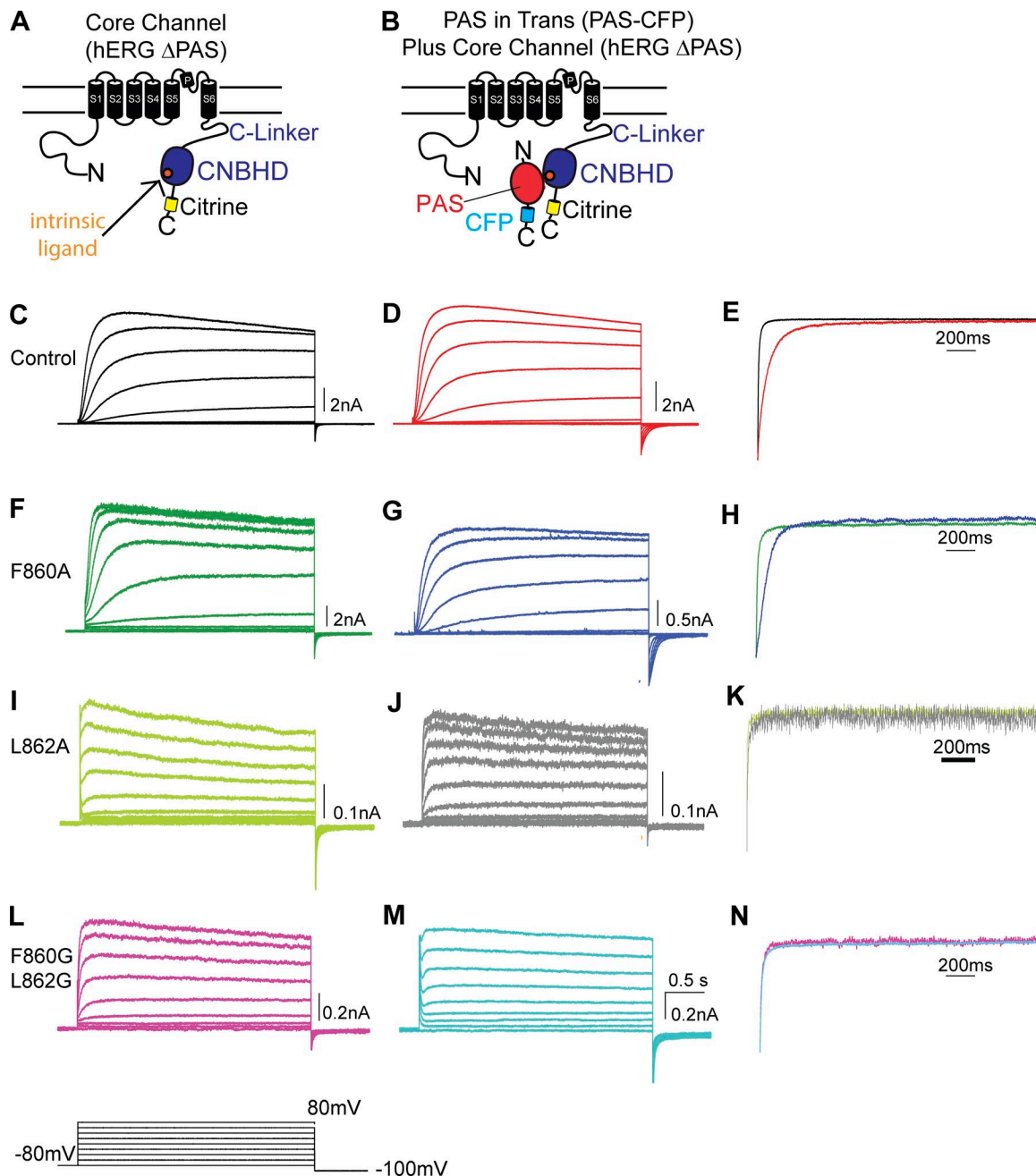
Figure 3. Mutations in the intrinsic ligand disrupted PAS domain–dependent regulation of slow deactivation gating. (A and B) Scheme of hERG core channels (A) and the PAS domain in trans with hERG core channels (B). **(C–E)** Whole-cell voltage-clamp recordings of a family of currents from positive control hERG core channels (C), positive control PAS domain in trans with hERG core channels (D), and overlay of tail currents from C and D at –100 mV (E). **(F–H)** Currents from hERG F860A core channels (F), the PAS domain in trans with hERG F860A core channels (G), and overlay of tail currents from F and G (H) . **(I–K)** Currents from hERG L862A core channels (I), the PAS domain in trans with hERG L862A core channels (J), and overlay of tail currents from I and J (K). **(L–N)** Currents from hERG F860G,L862G core channels (L), the PAS domain in trans with hERG F860G,L862G core channels (M), and overlay of tail currents from L and M (N). Voltage pulses used to elicit currents from a holding potential of –80 mV in 20-mV steps to 80 mV and repolarization to –100 mV, as indicated.

tioA – RatioA$_0$ near zero, indicating very little detectable FRET (Fig. 2 H). These results suggest that the F860A mutant perturbed a structural interaction between the PAS domain and the core of the channel and that the L862A mutant and the F860G,L862G double mutant prevented an interaction between the PAS domain and the CNBHD of the core channel. Our data indicate that the L862, more so than F860, determines the disruption of a PAS domain interaction with the core of the channel.

For each cell coexpressing PAS in trans with hERG core channels, we also measured the Fc/Fy ratio, which is an unbiased determination of the relative amount of donor to acceptor as measured from their relative fluorescence intensities (see Materials and methods; Eqs. 4–6). Fc/Fy was similar among the control PAS in trans with hERG core channels and the PAS in trans with hERG F860A, hERG core L862A or hERG core F860G,L862G mutant channels, as indicated (Fig. 2 I), meaning that the relative

Table 1. **Summary of electrophysiological measurements**

Construct	$V_{1/2}$	k	Time to half max (s)	Time to half max (SEM)	Time constant of deactivation 1 (ms)	Time constant of deactivation 1 (SEM)	Time constant of deactivation 2 (ms)	Time constant of deactivation 2 (SEM)
hERGΔPAS	16.1± 1.6 (3)	19.1 ± 1.5 (3)	0.35 (3)	0.0043	21.68 (4)	7.21	47.21 (3)	13.27
PAS + hERGΔPAS	10.9 ± 1.3 (3)	17.3 ± 1.2 (3)	0.32 (3)	0. 0091	72.43 (5)	6.73	201.47 (3)	10.00
WT	16.0 ± 0.9 (3)	16.2 ± 0.8 (3)	0.38 (4)	0.0236	96.00 (3)	8.19	205.01 (4)	23.16
hERG ΔPAS F860A	9.4 ± 3.00 (3)	22.6 ± 3.2 (3)	0.31 (3)	0.0069	15.97 (4)	2.42	119.61 (3)	24.23
PAS + hERGΔPAS F860A	8.5 ± 2.2 (3)	22.3 ± 2.3 (3)	0.33 (3)	0.0100	37.72 (3)	8.69	76.04 (3)	16.47
hERG ΔPAS L862A	−3.0 ± 3.7 (4)	18.7 ± 1.7 (4)	0.27 (3)	0.0037	4.59 (3)	1.97	38.96 (3)	14.49
PAS + hERG ΔPAS L862A	−5.0 ± 1.7 (3)	15.7 ± 2.0 (3)	0.25 (3)	0.0028	1.45 (3)	0.15	15.65 (3)	3.58
hERG ΔPAS F860G L862G	−6.6 ± 2.3 (3)	22.10 ± 2.4 (3)	0.25 (3)	0.0032	4.99 (3)	2.09	40.77 (3)	14.71
PAS + hERG ΔPAS F860G L862G	−3.0 ± 3.7 (3)	26.5 ± 4.3 (3)	0.25 (3)	0.0010	7.39 (3)	3.53	91.89 (3)	40.48

amounts of donor to acceptor were similar. This means that decreases in FRET were not simply due to too few donors, but rather indicate a bona fide reduction in FRET efficiency.

To investigate the function of channels with mutations in the intrinsic ligand, we performed whole-cell patch-clamp recordings of hERG channels expressed in HEK293 cells. We compared recordings from hERG core channels (Fig. 3 A) to channels formed from coexpression of the PAS domain in trans with hERG core channels (Fig. 3 B). The power of this assay is that we can compare channels with and without PAS domains and can attribute any measured differences to direct PAS domain interactions with the core of the channel (Gustina and Trudeau, 2009, 2013; Trudeau et al., 2011; Gianulis et al., 2013; Liu and Trudeau, 2015).

In positive control experiments, hERG core channels (Fig. 3 C) and the PAS domain in trans with hERG core channels (Fig. 3 D) had similar conductance–voltage relationships (Fig. 4 A) and activation properties (Fig. 5 C). But compared with hERG core channels, the PAS domain in trans with hERG core channels had slower deactivation (Fig. 3 E; Fig. 5, A and B; and Table 1), which means that the PAS domain regulates deactivation by a direct interaction with the core of the channel as previously reported (Gustina and Trudeau, 2009, 2013; Trudeau et al., 2011; Gianulis et al., 2013; Liu and Trudeau, 2015) and which is supported by the robust FRET between the PAS domain and hERG core (Fig. 2, D and H).

We measured hERG F860A core channels (Fig. 3 F) and compared them to PAS domains in trans with hERG F860A core channels (Fig. 3 G) and detected similar conductance–voltage relationships (Fig. 4 B) and activation properties (Fig. 5 C). PAS domains in trans with hERG F860A core channels had slower deactivation than hERG F860A core channels alone (Fig. 3 H; and Fig. 5, A and B), but deactivation was not as slow as in control channels, indicating a partial regulation of the hERG F860A core channels by the PAS domain (Fig. 5, A and B). This suggests that the PAS domain interaction with the core of the hERG channel was perturbed by F860A. This result is consistent with the partial change in FRET measured for PAS in trans with hERG F860A core

channels compared with the positive control of PAS in trans with core channels (Fig. 2 H).

Mutant hERG L862A core channels (Fig. 3 I) compared with PAS in trans with hERG L862A core channels (Fig. 3 J) had similar conductance relationships (Fig. 4 C) and similar activation
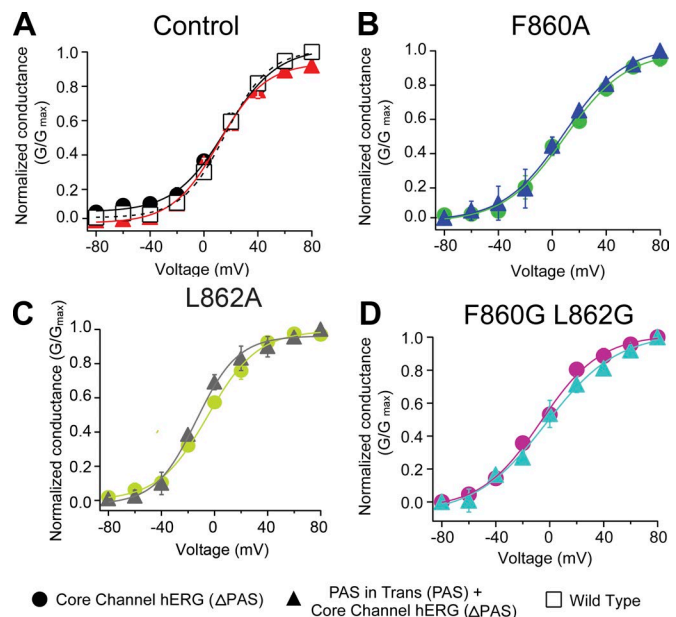

Figure 4. **Conductance–voltage relationships of hERG channels.** Plots of conductance versus voltage for hERG core channels (black closed circles, black trace), PAS domains in trans with hERG core channels (red closed triangles, red trace), and full-length WT hERG channels for comparison (open squares, dashed trace; A); hERG F860A core channels (green closed circle, green trace) and PAS domains in trans with hERG F860A core channels (blue closed triangles, blue trace; B); hERG L862A core channels (light green closed circle, light green trace) and PAS domains in trans with hERG L862A core channels (gray closed triangles, gray trace; C); and hERG F860G,L862G core channels (magenta closed circle, magenta trace) and PAS domains in trans with hERG F860G,L862G core channels (cyan closed triangles, cyan trace; D). Traces represent fits to a Boltzmann function. Points are the mean, and error bars are the SD. n = at least three for each; see Table 1.
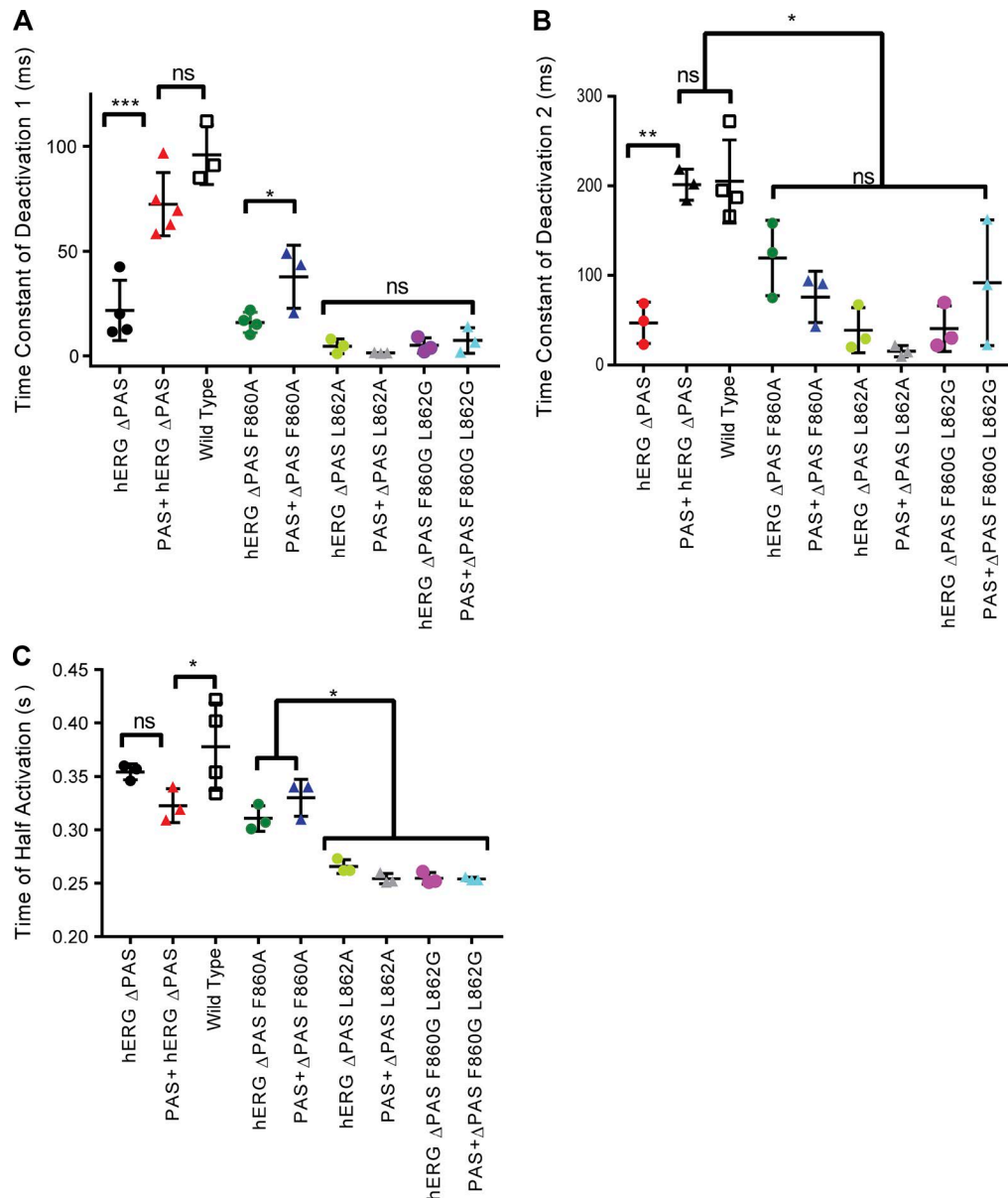
Figure 5. **Deactivation and activation time constants. (A)** Scatter plot of the fast time constant of deactivation (1) and **(B)** the slow time constant of deactivation (2) at –100 mV from data in Fig. 3. Deactivation was fit with a double exponential function. **(C)** Scatter plot of time to half-maximal activation of channels at 60 mV. ***, $P < 0.001$; **, $P < 0.01$; or *, $P < 0.05$ by one-way ANOVA and Tukey's post hoc test.

properties (Fig. 5 C). Deactivation was not measurably different between hERG L862 core channels and PAS in trans with hERG L862 core channels (Fig. 3 K; and Fig. 5, A and B). This result suggested that PAS domains did not measurably regulate core L862A channels, suggesting the lack of an interaction between the PAS domain and core L862A channels. This result is supported by the lack of measurable FRET between the PAS domain and hERG L862A core channels (Fig. 2, F and H).

We recorded from mutant hERG F860G,L862G core channels (Fig. 3 L) compared with PAS in trans with hERG F860G,L862G core channels (Fig. 3 M) and measured similar conductance relationships (Fig. 4 D) and similar activation properties (Fig. 5 C). Deactivation was not measurably different between hERG F860G,L862G core channels and PAS in trans with hERG F860G,L862G core channels (Fig. 3 N; and Fig. 5, A and B). This

result suggested that PAS domains did not measurably regulate hERG F860G,L862G core channels, suggesting the lack of an interaction between the PAS domain and hERG F860G,L862G core channels. This result is supported by the lack of measurable FRET between the PAS domain and hERG F860G,L862G core channels (Fig. 2, G and H).

Discussion

Here we show that point mutations in the hERG intrinsic ligand weaken or prevent functional regulation of hERG channel deactivation gating by the PAS domain as measured with electrophysiology and weaken or prevent a structural interaction of the PAS domain with the core of the channel as measured with FRET spectroscopy. The lack of a measurable change in channel deac-

tivation (Figs. 3; and Fig. 5, A and B) and the lack of measurable FRET (Fig. 2) for PAS in trans with core L862A channels and PAS in trans with hERG F860G,L862G core channels suggests that the intrinsic ligand is necessary for both the functional regulation of hERG by the PAS domain and for the structural interdomain PAS-CNBHD interaction. The intermediate amount of deactivation and intermediate FRET in channels containing PAS in trans with hERG F860A core channels indicates that this mutation lessened the functional regulation of core channels by the PAS domain and weakened the structural interaction of the PAS domain with the CNBHD. We interpret our results to mean that the intrinsic ligand mutants disrupted the PAS-CNBHD interaction and the regulation of deactivation gating in hERG channels (Fig. 6).

How these mutations alter the conformational landscape of the hERG CNBHD remains to be shown. The cryo-EM structures of hERG and the cocrystal structure of the EAG channel PAS-CNB HD domains show extensive buried surface at the PAS and CNBHD interaction, but the extent to which this surface is physiologically relevant has been tested only at a single site. A single mutation at a salt bridge between R56 in the PAS (R57 in EAG) and D803 (D642 in EAG) leads to a loss of the salt bridge, which alters gating (Haitin et al., 2013; Ng et al., 2014). In contrast, the intrinsic ligand does not appear to have such a specific interaction with the PAS domain. But the structures only represent one predominant state of the PAS-CNBHD interaction, or in the case of the cryo-EM structure, may not add additional clarity to identify new side-chain interactions at the interface in fine detail, so we cannot completely rule out a direct interaction of the intrinsic ligand and the PAS. Alternatively, our electrophysiology data shows that the intrinsic ligand mutations L862A and the double mutant F860G,L862G shift the GV curves to the left and speed up activation compared with F860A and positive control channels. These effects are similar to that of channels with deleted CNBHDs (Gustina and Trudeau, 2011; Gianulis et al., 2013) and suggests that the CNBHD may be more globally altered by the mutants, and as our results show, the CNBHD binds less or not at all to the PAS domain. Thus, allosteric regulation of the PAS-CNBHD interaction by the intrinsic ligand is the most consistent interpretation our data.

The PAS-CNBHD interaction and hERG deactivation gating is very sensitive to mutations at or near the PAS-CNBHD interface. In the CNBHD, as we show here, F860A lessened regulation and weakened the interaction of the PAS and the channel. Furthermore, L862A and the double mutant F860G,L862G had no measurable regulation of deactivation and FRET is near zero, indicating that these mutants prevent association of the PAS with the channel. The PAS domain mutant Y43A lessens regulation of deactivation and decreases FRET between the PAS and core of the channel, and the PAS domain mutant R56Q prevents regulation of deactivation and prevents FRET between the PAS and the core of the channel (Gustina and Trudeau, 2009). Despite the large number of structural contacts between the PAS and CNBHD (Haitin et al., 2013; Whicher and MacKinnon, 2016; Wang and MacKinnon, 2017), mutations at some PAS or CNBHD residues (e.g., R56 and L862) appear sufficient to prevent the interaction.

hERG and EAG channels may share structural dependence on the intrinsic ligand, although the intrinsic ligand appears to regulate different aspects of gating. In hERG channels that lack the
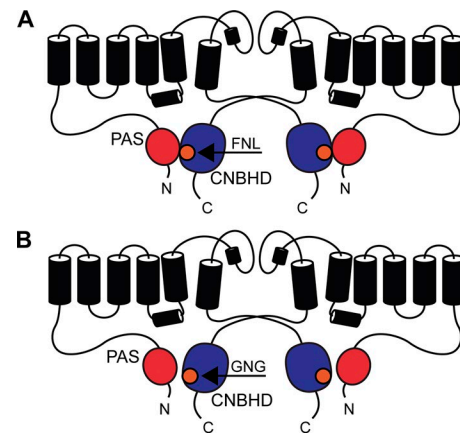

Figure 6. **Schematic of hERG channel PAS-CNBHD interaction and role of the intrinsic ligand. (A)** WT hERG channels showing the intrinsic ligand with intrinsic ligand residues FNL in the CNBHD and the PAS-CNBHD interaction. **(B)** Depiction of a hERG channel with the F860G,L862G double mutant in the intrinsic ligand showing a disruption of the PAS-CNBHD interaction. Two hERG subunits (of four) are shown for clarity.

CNBHD domain, deactivation and activation are faster than that in WT channels (Gustina and Trudeau, 2011; Gianulis et al., 2013). In contrast, deletion of the PAS domain speeds deactivation to the same extent as deletion of the CNBHD, but does not affect activation (Gustina and Trudeau, 2011; Gianulis et al., 2013). The interpretation of this result is that the CNBHD deletion speeds deactivation because the interaction with the PAS domain is prevented, but the speeding of activation is by an unknown mechanism. Here we report that hERG core L862A channels and hERG core F860G,L862G channels exhibited faster activation than that in control core hERG channels or hERG F860A core channels, indicating that the change in activation due to deletion of the CNB HD may be localized to the intrinsic ligand residue L862 (Fig. 5 C). Interestingly, a similar finding was reported in EAG channels, where EAG channels with a double mutation of Y699G,L701G in the intrinsic ligand are phenocopies of EAG channels with a deletion of the CNBHD, as both channels have slowed activation properties and lack the Cole–Moore shift (Zhao et al., 2017). Thus, hERG (this study) and EAG channels (Zhao et al., 2017) share the feature that channels with intrinsic ligand mutants are phenocopies of channels with deletion of the entire CNBHD.

The intrinsic ligand appears to have some intriguing differences and similarities among the KCNH channels. In ELK channels, deletion of the YNL motif or mutations in the YNL motif disrupt voltage-dependent potentiation, a feature where depolarizing prepulses increase current amplitude and hyperpolarize the conductance–voltage relationship (Dai and Zagotta, 2017; Dai et al., 2018). Transition metal FRET studies indicated that the Y in ELK channels moves relative to a transition metal ion bound to a di-histidine motif in the ELK PAS domain (Dai and Zagotta, 2017) or the CNBHD (Dai et al., 2018), indicating a movement of the intrinsic ligand with voltage. Like ELK channels (Dai et al., 2018), hERG channels may also exhibit a voltage-dependent potentiation. But in hERG, the voltage-dependent potentiation may occur much faster than for ELK and appears to lead to the slow deactivation in hERG (Ng et al., 2011; Goodchild et al., 2015).

While mutations in hERG at the intrinsic ligand motif sped up channel deactivation, they did so without an apparent shift in the conductance–voltage relationship in full-length hERG channels (Brelidze et al., 2013), in contrast to that in ELK channels (Dai and Zagotta, 2017). Here we report that intrinsic ligand mutations perturb hERG deactivation and disrupt the PAS-CNBHD interaction. Thus, the ELK and ERG intrinsic ligand motifs may play somewhat similar roles. In human EAG channels, the YNL motif is required for the Cole–Moore shift, in which the activation rate of EAG depends on the prepulse voltage (Zhao et al., 2017), but neither hERG nor ELK channels have a measurable Cole–Moore shift (Trudeau et al., 1999). Thus, the mechanistic role for the intrinsic ligand appears to have some functional similarities between hERG and ELK, but EAG channels appear somewhat distinct. Future studies may delineate whether the intrinsic ligand mechanism is indeed fundamentally different or similar among the KCNH channels.

Acknowledgments

References

Bianchi, L., B. Wible, A. Arcangeli, M. Taglialatela, F. Morra, P. Castaldo, O. Crociani, B. Rosati, L. Faravelli, M. Olivotto, and E. Wanke. 1998. herg encodes a K+ current highly conserved in tumors of different histogenesis: a selective advantage for cancer cells? *Cancer Res.* 58:815–822.

Brelidze, T.I., A.E. Carlson, and W.N. Zagotta. 2009. Absence of direct cyclic nucleotide modulation of mEAG1 and hERG1 channels revealed with fluorescence and electrophysiological methods. *J. Biol. Chem.* 284:27989–27997. https://doi.org/10.1074/jbc.M109.016337

Brelidze, T.I., A.E. Carlson, B. Sankaran, and W.N. Zagotta. 2012. Structure of the carboxy-terminal region of a KCNH channel. *Nature.* 481:530–533. https://doi.org/10.1038/nature10735

Brelidze, T.I., E.C. Gianulis, F. DiMaio, M.C. Trudeau, and W.N. Zagotta. 2013. Structure of the C-terminal region of an ERG channel and functional implications. *Proc. Natl. Acad. Sci. USA.* 110:11648–11653. https://doi.org/10.1073/pnas.1306887110

Curran, M.E., I. Splawski, K.W. Timothy, G.M. Vincent, E.D. Green, and M.T. Keating. 1995. A molecular basis for cardiac arrhythmia: HERG mutations cause long QT syndrome. *Cell.* 80:795–803. https://doi.org/10.1016/0092-8674(95)90358-5

Dai, G., and W.N. Zagotta. 2017. Molecular mechanism of voltage-dependent potentiation of KCNH potassium channels. *eLife.* 6:e26355. https://doi.org/10.7554/eLife.26355

Dai, G., Z.M. James, and W.N. Zagotta. 2018. Dynamic rearrangement of the intrinsic ligand regulates KCNH potassium channels. *J. Gen. Physiol.* 150:625–635. https://doi.org/10.1085/jgp.201711989

Erickson, M.G., B.A. Alseikhan, B.Z. Peterson, and D.T. Yue. 2001. Preassociation of calmodulin with voltage-gated Ca(2+) channels revealed by FRET in single living cells. *Neuron.* 31:973–985. https://doi.org/10.1016/S0896-6273(01)00438-X

Gianulis, E.C., and M.C. Trudeau. 2011. Rescue of Aberrant Gating by a Genetically-Encoded PAS (Per-Arnt-Sim) Domain in Several Long QT Syndrome Mutant Human ERG (hERG) Potassium Channels. *J. Biol. Chem.* 286:22160–22169. https://doi.org/10.1074/jbc.M110.205948

Gianulis, E.C., Q. Liu, and M.C. Trudeau. 2013. Direct interaction of eag domains and cyclic nucleotide-binding homology domains regulate deactivation gating in hERG channels. *J. Gen. Physiol.* 142:351–366. https://doi.org/10.1085/jgp.201310995

Goodchild, S.J., L.C. Macdonald, and D. Fedida. 2015. Sequence of gating charge movement and pore gating in HERG activation and deactivation pathways. *Biophys. J.* 108:1435–1447. https://doi.org/10.1016/j.bpj.2015.02.014

Guasti, L., E. Cilia, O. Crociani, G. Hofmann, S. Polvani, A. Becchetti, E. Wanke, F. Tempia, and A. Arcangeli. 2005. Expression pattern of the ether-a-go-go-related (ERG) family proteins in the adult mouse central nervous system: evidence for coassembly of different subunits. *J. Comp. Neurol.* 491:157–174. https://doi.org/10.1002/cne.20721

Gustina, A.S., and M.C. Trudeau. 2009. A recombinant N-terminal domain fully restores deactivation gating in N-truncated and long QT syndrome mutant hERG potassium channels. *Proc. Natl. Acad. Sci. USA.* 106:13082–13087. https://doi.org/10.1073/pnas.0900180106

Gustina, A.S., and M.C. Trudeau. 2011. hERG potassium channel gating is mediated by N- and C-terminal region interactions. *J. Gen. Physiol.* 137:315–325. https://doi.org/10.1085/jgp.201010582

Gustina, A.S., and M.C. Trudeau. 2012. HERG potassium channel regulation by the N-terminal eag domain. *Cell. Signal.* 24:1592–1598. https://doi.org/10.1016/j.cellsig.2012.04.004

Gustina, A.S., and M.C. Trudeau. 2013. The eag domain regulates hERG channel inactivation gating via a direct interaction. *J. Gen. Physiol.* 141:229–241. https://doi.org/10.1085/jgp.201210870

Guy, H.R., S.R. Durell, J. Warmke, R. Drysdale, and B. Ganetzky. 1991. Similarities in amino acid sequences of Drosophila eag and cyclic nucleotide-gated channels. *Science.* 254:730. https://doi.org/10.1126/science.1658932

Haitin, Y., A.E. Carlson, and W.N. Zagotta. 2013. The structural mechanism of KCNH-channel regulation by the eag domain. *Nature.* 501:444–448. https://doi.org/10.1038/nature12487

Herzberg, I.M., M.C. Trudeau, and G.A. Robertson. 1998. Transfer of rapid inactivation and sensitivity to the class III antiarrhythmic drug E-4031 from HERG to M-eag channels. *J. Physiol.* 511:3–14. https://doi.org/10.1111/j.1469-7793.1998.003bi.x

James, Z.M., and W.N. Zagotta. 2017. Structural insights into the mechanisms of CNBD channel function. *J. Gen. Physiol.* 150:225–244. https://doi.org/10.1085/jgp.201711898

Jones, D.K., A.C. Johnson, E.C. Roti Roti, F. Liu, R. Uelmen, R.A. Ayers, I. Baczko, D.J. Tester, M.J. Ackerman, M.C. Trudeau, and G.A. Robertson. 2018. Localization and functional consequences of a direct interaction between TRIOBP-1 and hERG proteins in the heart. *J. Cell Sci.* 131:jcs206730. https://doi.org/10.1242/jcs.206730

Khoo, K.K., and S.A. Pless. 2018. How an intrinsic ligand tunes the activity of a potassium channel. *J. Gen. Physiol.* 150:517–520. https://doi.org/10.1085/jgp.201812011

Liu, Q.N., and M.C. Trudeau. 2015. Eag Domains Regulate LQT Mutant hERG Channels in Human Induced Pluripotent Stem Cell-Derived Cardiomyocytes. *PLoS One.* 10:e0123951. https://doi.org/10.1371/journal.pone.0123951

Morais Cabral, J.H., A. Lee, S.L. Cohen, B.T. Chait, M. Li, and R. Mackinnon. 1998. Crystal structure and functional analysis of the HERG potassium channel N terminus: a eukaryotic PAS domain. *Cell.* 95:649–655. https://doi.org/10.1016/S0092-8674(00)81635-9

Morais-Cabral, J.H., and G.A. Robertson. 2015. The enigmatic cytoplasmic regions of KCNH channels. *J. Mol. Biol.* 427:67–76. https://doi.org/10.1016/j.jmb.2014.08.008

Ng, C.A., M.J. Hunter, M.D. Perry, M. Mobli, Y. Ke, P.W. Kuchel, G.F. King, D. Stock, and J.I. Vandenberg. 2011. The N-terminal tail of hERG contains an amphipathic α-helix that regulates channel deactivation. *PLoS One.* 6:e16191. https://doi.org/10.1371/journal.pone.001619

Ng, C.A., K. Phan, A.P. Hill, J.I. Vandenberg, and M.D. Perry. 2014. Multiple interactions between cytoplasmic domains regulate slow deactivation of Kv11.1 channels. *Journal of Biological Chemistry*. 289:25822–25832. https://doi.org/10.1074/jbc.M114.558379

Rizzo, M.A., G. Springer, K. Segawa, W.R. Zipfel, and D.W. Piston. 2006. Optimization of pairings and detection conditions for measurement of FRET between cyan and yellow fluorescent proteins. *Microsc. Microanal.* 12:238–254. https://doi.org/10.1017/S1431927606060235

Robertson, G.A., J.M. Warmke, and B. Ganetzky. 1996. Potassium currents expressed from Drosophila and mouse eag cDNAs in Xenopus oocytes. *Neuropharmacology*. 35:841–850. https://doi.org/10.1016/0028-3908(96)00113-X

Sanguinetti, M.C., and N.K. Jurkiewicz. 1990. Two components of cardiac delayed rectifier K+ current. Differential sensitivity to block by class III antiarrhythmic agents. *J. Gen. Physiol.* 96:195–215. https://doi.org/10.1085/jgp.96.1.195

Sanguinetti, M.C., C. Jiang, M.E. Curran, and M.T. Keating. 1995. A mechanistic link between an inherited and an acquired cardiac arrhythmia: HERG encodes the IKr potassium channel. *Cell*. 81:299–307. https://doi.org/10.1016/0092-8674(95)90340-2

Selvin, P.R. 1995. Fluorescence resonance energy transfer. *Methods Enzymol.* 246:300–334. https://doi.org/10.1016/0076-6879(95)46015-2

Shaner, N.C., P.A. Steinbach, and R.Y. Tsien. 2005. A guide to choosing fluorescent proteins. *Nat. Methods.* 2:905–909. https://doi.org/10.1038/nmeth819

Trudeau, M.C., and W.N. Zagotta. 2004. Dynamics of Ca2+-calmodulin-dependent inhibition of rod cyclic nucleotide-gated channels measured by patch-clamp fluorometry. *J. Gen. Physiol.* 124:211–223. https://doi.org/10.1085/jgp.200409101

Trudeau, M.C., J.W. Warmke, B. Ganetzky, and G.A. Robertson. 1995. HERG, a human inward rectifier in the voltage-gated potassium channel family. *Science.* 269:92–95. https://doi.org/10.1126/science.7604285

Trudeau, M.C., S.A. Titus, J.L. Branchaw, B. Ganetzky, and G.A. Robertson. 1999. Functional analysis of a mouse brain Elk-type K+ channel. *J. Neurosci.* 19:2906–2918. https://doi.org/10.1523/JNEUROSCI.19-08-02906.1999

Trudeau, M.C., L.M. Leung, E.R. Roti, and G.A. Robertson. 2011. hERG1a N-terminal eag domain-containing polypeptides regulate homomeric hERG1b and heteromeric hERG1a/hERG1b channels: a possible mechanism for long QT syndrome. *J. Gen. Physiol.* 138:581–592. https://doi.org/10.1085/jgp.201110683

Wang, W., and R. MacKinnon. 2017. Cryo-EM Structure of the Open Human Ether-à-go-go-Related K$^+$ Channel hERG. *Cell.* 169:422–430.e10. https://doi.org/10.1016/j.cell.2017.03.048

Warmke, J.W., and B. Ganetzky. 1994. A family of potassium channel genes related to eag in Drosophila and mammals. *Proc. Natl. Acad. Sci. USA.* 91:3438–3442. https://doi.org/10.1073/pnas.91.8.3438

Warmke, J., R. Drysdale, and B. Ganetzky. 1991. A distinct potassium channel polypeptide encoded by the Drosophila eag locus. *Science.* 252:1560–1562. https://doi.org/10.1126/science.1840699

Whicher, J.R., and R. MacKinnon. 2016. Structure of the voltage-gated K$^+$ channel Eag1 reveals an alternative voltage sensing mechanism. *Science.* 353:664–669. https://doi.org/10.1126/science.aaf8070

Zagotta, W.N., N.B. Olivier, K.D. Black, E.C. Young, R. Olson, and E. Gouaux. 2003. Structural basis for modulation and agonist specificity of HCN pacemaker channels. *Nature.* 425:200–205. https://doi.org/10.1038/nature01922

Zhao, Y., M.P. Goldschen-Ohm, J.H. Morais-Cabral, B. Chanda, and G.A. Robertson. 2017. The intrinsically ligaded cyclic nucleotide-binding homology domain promotes KCNH channel activation. *J. Gen. Physiol.* 149:249–260. https://doi.org/10.1085/jgp.201611701

Zheng, J., and W.N. Zagotta. 2004. Stoichiometry and assembly of olfactory cyclic nucleotide-gated channels. *Neuron.* 42:411–421. https://doi.org/10.1016/S0896-6273(04)00253-3